Spiroindoline-Capped Selective HDAC6 Inhibitors: Design, Synthesis, Structural Analysis, and Biological Evaluation

NOVEL SPIROINDOLINE-CAPPED SELECTIVE HDAC6 INHIBITORS: DESIGN, SYNTHESIS, STRUCTURAL ANALYSIS AND BIOLOGICAL EVALUATION

A. Prasanth Saraswati,[a,#] Nicola Relitti,[a,#] Jeremy D. Osko,[b] Giulia Chemi,[a,1] Stefano Federico,[a] Alessandro Grillo,[a,2] Simone Brogi,[c] Niamh H. McCabe,[d] Richard C. Turkington,[d] Ola Ibrahim,[e] Jeffrey O'Sullivan,[e] Stefania Lamponi,[a] Magda Ghanim,[f] Vincent P. Kelly,[f] Daniela Zisterer+student,[f] Francesca Vanni,[g] Cristina Ulivieri,[g] Daniel Herp,[h] Antonella Di Costanzo,[i] Fulvio Saccoccia,[j] Giovina Ruberti,[j] Manfred Jung,[h] Lucia Altucci,[i] Sandra Gemma,[a] Stefania Butini[a], Christianson David W,[b] Margherita Brindisi,[k] Giuseppe Campiani[a,*]

[a]University of Siena, Department of Biotechnology, Chemistry and Pharmacy, DoE Department of Excellence 2018-2022, via Aldo Moro 2, I-53100 Siena, Italy

[b]Roy and Diana Vagelos Laboratories, Department of Chemistry, University of Pennsylvania, Philadelphia, PA, United States

[c]Department of Pharmacy, University of Pisa, via Bonanno 6, 56126, Pisa, Italy

[d]Centre for Cancer Research and Cell Biology, Queens University Belfast, Belfast, UK

[e]School of Dental Science, Trinity College Dublin, Lincoln Place, Dublin 2, Ireland

[f]School of Biochemistry and Immunology, Trinity Biomedical Science Institute, Trinity College, 152-160, Pearse Street, Dublin 2, Ireland

[g] Department of Life Sciences, University of Siena, via Aldo Moro 2, I-53100 Siena, Italy

[h]Institute of Pharmaceutical Sciences, Albert-Ludwigs-Universität Freiburg, Albertstraße 25, 79104, Freiburg, Germany

[i]Department of Precision Medicine, University of Campania "Luigi Vanvitelli", 80138 Naples, Italy

[j]Institute of Biochemistry and Cell Biology (IBBC), National Research Council (CNR), via E. Ramarini 32, 00015 Monterotondo (Rome), Italy

[k]University of Napoli Federico II, Department of Pharmacy, DoE Department of Excellence 2018-2022, via D. Montesano 49, I-80131 Napoli, Italy

KEYWORDS: *HDAC6, isoform-selective, spiroindoline, cancer therapy, STAT3*

ABSTRACT: Histone deacetylase inhibitors (HDACi) have emerged as promising therapeutics for the treatment of neurodegeneration, cancer and rare disorders. Herein, we report the development of a series of spiroindoline derivatives as novel HDAC6 isoform-selective inhibitors based on the X-ray crystal studies of the prototype compound **6a**. On investigating the inhibition profile of this series of compounds against recombinant HDAC enzymes, we identified compound **6j** as the most selective and potent *h*HDAC6 inhibitor with an IC_{50} value of 48.5 nM and a selectivity index of 140 over *h*HDAC1 and 66 over *h*HDAC8. Further biological evaluation on compounds **6b**, **6h** and **6j** demonstrated antiproliferative activity in the micromolar range against diverse cancer cell lines. Western blotting studies indicated that **6b** and **6h** were

able to increase tubulin acetylation, and **6h** induced PARP cleavage indicating its apoptotic potential at the molecular level while **6j** displayed pSTAT3 inhibition which is in turn regulated by inhibition of HDAC6.

GRAPHICAL ABSTRACT:

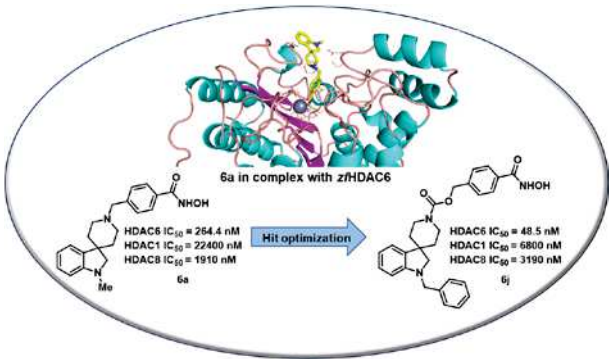

Many human diseases have an underlying epigenetic etiology, including cancer, diabetes, cardiovascular, neurological and metabolic disorders.[1] In eukaryotic cells, histone proteins play a crucial role in organizing the DNA into structures called nucleosomes. Histone acetylation and deacetylation comprises a prime example of post-translational modifications (PTM) that function in epigenetic regulation. Histone deacetylases (HDAC) belong to the family of hydrolases that remove acetyl groups from lysine residues and thereby regulate key processes such as gene expression.[2] They are clustered in 4 different classes (I-IV) based on their homology to yeast HDACs. Class I HDAC enzymes consist of isoforms 1, 2, 3 and 8; whereas class II, enzymes include the isoforms 4, 5, 6, 7, 9, and 10. Class IV contains only isoform 11 and similar to class I and II this enzyme is zinc dependent. In contrast, the class III HDACs are NAD^+ dependent enzymes called sirtuins (SIRT isoforms 1-7). A common general structural feature of HDAC inhibitors (HDACi) is the presence of a zinc binding group (ZBG), a linker moiety and a cap group portion. Both the linker and the cap-group can be functionalized to modulate selectivity towards specific HDAC isoforms.[3] Many HDACi have been identified as therapeutic tools in the treatment of various disorders such as cancer, infectious diseases, neurodegenerative diseases and rare disorders.[4–6] To date, four HDACi have been approved by the FDA in cancer therapy: vorinostat (SAHA, **1**) and romidepsin (**2**) for cutaneous T-cell lymphomas treatment (CTCL),[7,8] panobinostat (**3**) for multiple myeloma,[9] and belinostat (**4**) for relapsed or refractory peripheral T-cell lymphoma[10] (Figure **1**). Unfortunately, these HDACi have proven to be non-selective or only partially selective and their use may lead to several unwanted side-effects.[11]

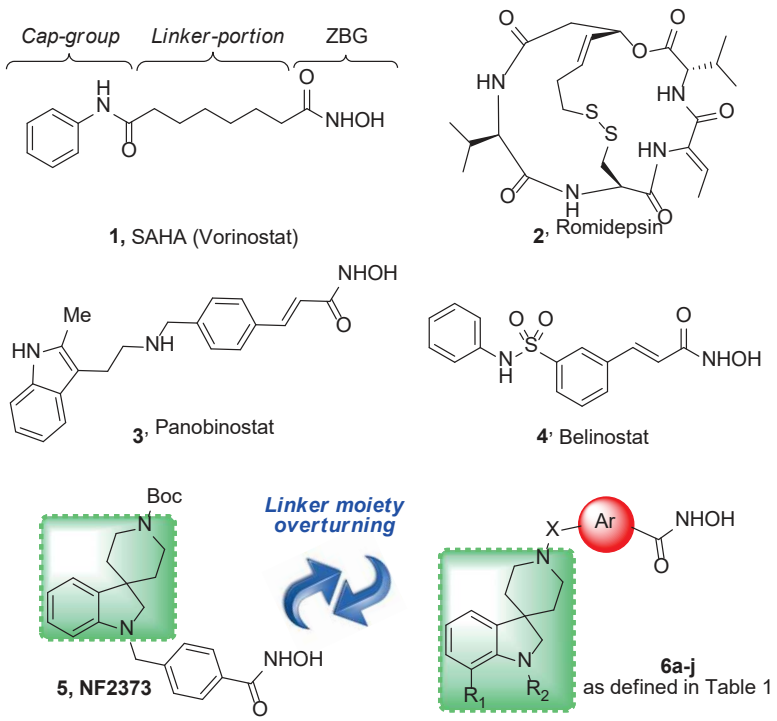

Figure 1. Structure of SAHA (**1**), romidepsin (**2**), panobinostat (**3**), belinostat (**4**), previously developed spiroindoline inhibitor (**5**) and novel HDAC6 inhibitors **6a-j**.

Significant research efforts are currently focused on the development of isoform-selective HDACi in the treatment of various diseases that lack the undesirable side effects of existent pan-HDAC drug candidates. In this regard, many recent efforts from the scientific community aimed at developing selective HDAC6i.[12] HDAC6 represents a unique member of the HDAC family due to two main factors: a) it contains two distinct catalytic domains and is primarily found in the cytoplasm (unlike HDAC1, 2 and 3, which are nuclear localized isoforms and HDAC8, which displays both nuclear and cytoplasmic distribution); b) it predominantly acts on non-histone substrates, such as α-tubulin, Hsp90 and cortactin.[13] Aiming at developing novel anticancer agents we directed our attention toward the HDAC6 because of its known involvement in cancer cell migration and metastasis.[14] The contribution of non-histone proteins such as α-tubulin and Hsp90 in HDAC6-mediated tumorigenesis makes HDAC6 inhibition a unique therapeutic strategy for cancer chemotherapy, with respect to the use of classical pan-HDAC inhibitors.[15] Interestingly, the cytosolic enzyme HDAC10, which is closely related to HDAC6, is mainly known to promote autophagy-mediated effects and is ineffective as a lysine deacetylase.[16]

In an effort to develop potent and selective HDAC6i, our group has recently identified a highly potent and selective spiroindoline-capped HDACi (**5**, NF2373, Figure **1**) which exhibited promising anticancer activity against several cancer cell lines.[17] This previous work allowed us to ascertain the spiroindoline scaffold as an optimal cap group for selective HDAC6 inhibition. In this work, we have investigated the impact of a strategical overturning of the linker and the ZBG moieties from the indoline nitrogen (as in compound **5**) to the piperidine nitrogen (compounds **6a-j**). The prototype of this novel series of compounds (**6a**, Table 1) demonstrated a promising HDAC6 IC_{50} value of 264.4 nM with a selectivity index of 85 over HDAC1 and 7

over *h*HDAC8. To get a deeper understanding of the binding mode of this compound, a 2.09 Å-resolution X-ray crystal structure was determined of the complex between **6a** and catalytic domain 2 of HDAC6 from *Danio rerio* (zebrafish). The active site structure of zebrafish HDAC6 is essentially identical to that of human HDAC6, and zebrafish HDAC6 yields crystals of much better quality compared with crystals of human HDAC6.[18] Subsequently, molecular modeling approaches were exploited to analyze the binding mode and the structural requirements to design novel "reversed" spiroindolines with an improved HDAC6 inhibitory profile and selectivity index. This was achieved following two main strategies: i) synthesizing derivatives with bulkier cap-groups, and ii) modulating the outdistancing between the cap-group and the ZBG, through the insertion of amide, urea and carbamate functionalities in the linker portion. The resulting compounds (**6b-j**) were tested for their ability to inhibit the HDAC1, 6 and 8 isoforms. In addition, the best performing compounds were further evaluated for their effects on cell cycle progression and apoptosis in various cancer cell lines.

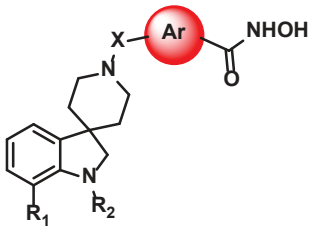

Table 1. Inhibitory activity of compounds **6a-j** and reference compounds (**5** and tubastatin A) against *h*HDAC1, as IC_{50} (μM), and *h*HDAC6, as IC_{50} (nM).

Cpd	R_1	R_2	X	Ar	HDAC1 IC_{50} (μM)[a] or % of inhibition at 1 μM	HDAC6 IC_{50} (nM)[a] or % of inhibition at 1 μM	HDAC1/HDAC6
6a NF2657	H	$-CH_3$	$-CH_2-$	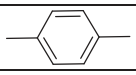	22.4 ± 6	264.4 ± 45	85
6b NF2864	H	$-CH_2C_6H_5$	$-CH_2-$	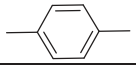	6.5 ± 0.8	561.0 ± 203	12
6c NF2872	H	$-COC_6H_5$	$-CH_2-$	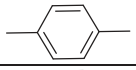	10.1 ± 2.1	155.0 ± 26	65
6d NF2876	C_6H_5	$-CH_3$	$-CH_2-$	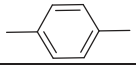	8.5%	50.0%	n.d.
6e NF2875	C_6H_5	$-CH_2C_6H_5$	$-CH_2-$	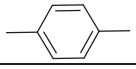	2.9%	29.7%	n.d.
6f NF2877	C_6H_5	$-COC_6H_5$	$-CH_2-$	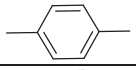	4.7 ± 0.5	465.0 ± 122	10
6g NF2865	H	$-CH_3$	$-CH_2-$	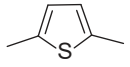	6.6 %	51.3%	n.d.
6h NF2867	H	$-CH_2C_6H_5$	$-COCH_2-$	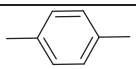	10.2 ± 1	227.0 ± 97	45
6i NF2870	H	$-CH_2C_6H_5$	$-CONHCH_2-$	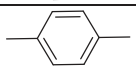	3.6 ± 0.3	110.0 ± 19	33
6j NF2866	H	$-CH_2C_6H_5$	$-COOCH_2-$	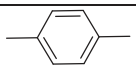	6.8 ± 0.3	48.5 ± 23	140
5[17]	-	-	-	-	4.00 ± 0.78	41.9 ± 7.9	95
Tubastatin A	-	-	-	-	1.91 ± 0.42	30.4 ± 2.1	63

[a]All compounds were assayed at least two times, and the results are expressed with standard deviations.

For the synthesis of compounds **6a-j**, four key-steps were employed to obtain the desired products which include: i) a Fischer indole synthesis, starting from suitable arylhydrazines and *N*-Boc-piperidine-4-carboxaldehyde providing 3,3-disubstituted indolenines, ii) reduction of the imine bond of the indolenines to get the respective indolines, iii) appropriate substitution at the *N*-1 position of the indoline, and, iv) insertion at the piperidine nitrogen with suitable linkers.

Scheme 1.A describes the synthesis of compounds **6a-f**. Commercially available 1-Boc-4-piperidone (**7**) was converted to its enol ether derivative by Wittig reaction using (methoxymethyl)triphenylphosphonium chloride in the presence of NaHMDS as the base.[19] The corresponding enol ether was hydrolyzed with cerium(III)chloride in MeCN to obtain **8** in high yield. Compound **8** and the suitable phenyl hydrazine were heated in AcOH at 80 ºC to obtain the corresponding spiroindolenines, by applying a Fischer indole synthetic protocol.[20,21] These intermediates were then reduced by catalytic hydrogenation to provide the spiroindolines **9a** and **9b**. A reductive amination of these latter with the suitable aldehydes in the presence of $NaBH_3CN$ or treatment with benzoyl chloride in the presence of TEA afforded the *N*-substituted derivatives, which, upon Boc-deprotection, provided amines **10a-f**. A second reductive amination protocol, performed on the piperidine using methyl 4-formyl benzoate followed by treatment of the resulting ester derivatives with NH_2OH and aqueous KOH, afforded the desired compounds **6a** and **6b-f**.

Scheme 1. Synthesis of the final compounds 6a-j[a]

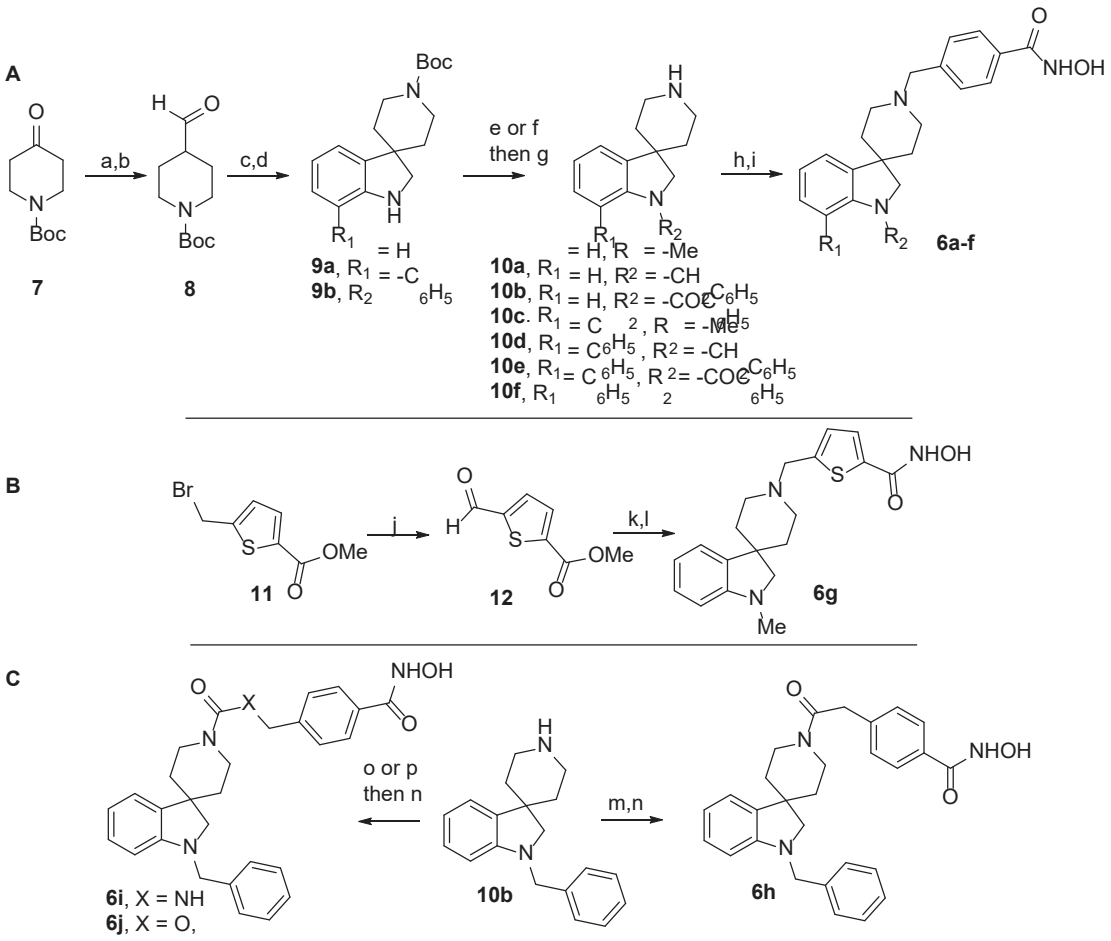

[a]Reagents and conditions: (A) a) $Ph_3P(Cl)CH_2OMe$, NaHMDS, THF, 0 to 25 ºC, 30 min; b) $CeCl_3 \cdot 7H_2O$, NaI, 40 ºC, MeCN, 16 h; c) phenylhydrazine or (1,1-biphenyl)-2-ylhydrazine·HCl , AcOH, 80 ºC, 2 h; d) H_2, Pd/C, MeOH, 25 ºC, 3 h; e) paraformaldehyde or benzaldehyde, $NaBH_3CN$, MeOH, 25 ºC, 8 h; f) benzoyl chloride, TEA, DCM, 25 ºC, 1 h; g) 1 N HCl in MeOH, 25 ºC, 15 min; h) methyl 4-formyl benzoate, $NaBH_3CN$, MeOH, 25 ºC, 8 h; i) NH_2OH (50% wt in H_2O), 4 M KOH in MeOH, DCM/MeOH, 25 ºC, 2 h.

(C) j) NMO, MeCN, 25 ºC, 12 h; k) **10a**, $NaBH_3CN$, MeOH, 25 ºC, 8 h; l) NH_2OH (50% in H_2O), KOH, DCM, MeOH, 25 ºC, 2 h.

(B) m) 2-(4-(Methoxycarbonyl)phenyl)acetic acid, EDCI, HOBt, DIPEA, DCM, 0º to 25 ºC, 24 h; n) NH_2OH (50% in H_2O), KOH, DCM, MeOH, 25 ºC, 2 h; o) methyl 4-(isocyanatomethyl)benzoate, TEA, dry THF, 45 ºC, 2 h; p) methyl 4-(hydroxymethyl)benzoate, CDI, DCM, 0º to 25 ºC, 6 h;

Thiophene-based compound **6g** was synthesized as described in Scheme 1.B. Aldehyde **12** was obtained from the bromo derivative **11** upon reaction with 4-methylmorpholine *N*-oxide (NMO) in MeCN.[17] The successive reductive amination reaction involving **10a** and **12** afforded the methyl ester intermediate, which was converted to the hydroxamate **6g**.

For the synthesis of the amide derivative **6h** (Scheme 1.C), 2-(4-(methoxycarbonyl)phenyl)acetic acid (synthesized as described in the supporting information, Scheme 1 SI) was coupled with amine **10b** and the resulting methyl ester intermediate was converted to the corresponding hydroxamic acid **6h**. To synthesize the urea **6i**, the key intermediate was methyl 4-(isocyanatomethyl)benzoate (see supporting information, Scheme 1 SI) which was reacted with **10b** to obtain the methyl ester intermediate subsequently converted to the hydroxamic acid **6i**. Finally, the carbamate **6j** was prepared by reacting amine **10b** with the commercially available methyl 4-(hydroxymethyl)benzoate in the presence of CDI in DCM to afford the methyl ester intermediate needed for subsequent conversion into the corresponding hydroxamic acid **6j**.

The 2.09 Å-resolution crystal structure of the HDAC6 CD2-**6a** complex reveals that the inhibitor hydroxamate group coordinates to the catalytic Zn^{2+} ion with a bidentate geometry (Figure 2). The Zn^{2+}-bound hydroxamate C=O group accepts a hydrogen bond from Y745, the Zn^{2+}-bound hydroxamate N-O^- group accepts a hydrogen bond from H573, and the hydroxamate NH group donates a hydrogen bond to H574. This constellation of intermolecular interactions with catalytically important residues accounts for the generally high affinity of hydroxamate-based inhibitors in the HDAC6 active site.

The *para*-substituted phenyl linker makes favorable offset π-π interactions in the aromatic crevice defined by F583 and F643. The piperidine ring adopts a chair conformation and the piperidine nitrogen forms a hydrogen bond with a water molecule that in turn hydrogen bonds with the backbone carbonyl of R798. The spiroindoline capping group is oriented toward the L2 pocket at the mouth of the active site. There, the indoline nitrogen hydrogen bonds with a water molecule that in turn hydrogen bonds with N645 and a second water molecule; a third water molecule completes a hydrogen bond network between the indoline nitrogen and Zn^{2+} ligand H614. Although the inhibitor makes no direct enzyme-inhibitor hydrogen bonds apart from those made with the hydroxamate moiety, it is interesting that three water molecules comprise a "wet" hydrogen bonded interface in such a high-affinity enzyme-inhibitor pair.

It is relatively rare to see inhibitor capping groups bind in the L2 pocket, since most tend to bind in the L1 pocket on the opposite side of the active site.[12,22–25] It appears that the chair conformation of the piperidine ring combined with the molecular structure of the novel spiro-fused indoline moiety yields a structure and a conformation that is ideal for binding within the L2 pocket.

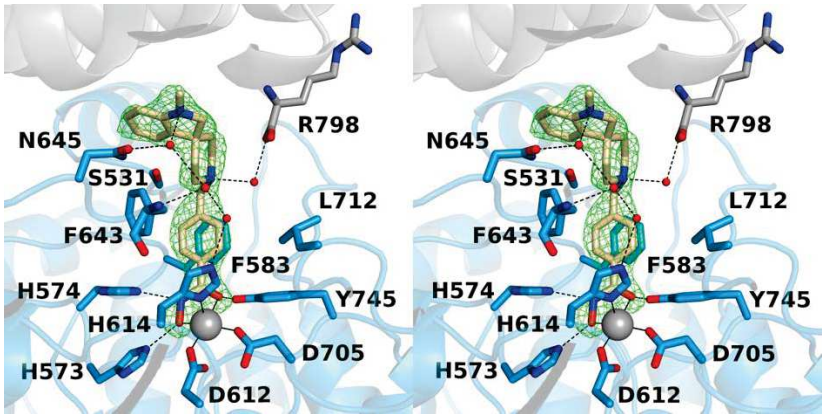

Figure 2. Stereoview of a Polder omit map of the HDAC6-**6a** complex for which the atomic coordinates of **6a** were omitted from the structure factor calculation (PDB 6V7A; contoured at 5.0 σ). Atoms are color-coded as follows: C = light blue (HDAC6 catalytic domain 2), light gray (symmetry mate), or wheat (inhibitor), N = blue, O = red, Zn^{2+} = gray sphere, and solvent = small red spheres. Metal coordination and hydrogen bond interactions are indicated by solid and dashed black lines, respectively.

The *in vitro* inhibitory profile of the newly developed compounds **6a-j** (Table 1) was evaluated against both *h*HDAC1 and 6 isoforms. SAR studies were performed by taking into consideration the data obtained from *in vitro*, X-ray and computational studies. These calculations outlined the preferential binding of the "reversed" spiroindoline compounds towards HDAC6. To get a better understanding of the behavior of the compounds in the binding sites of *h*HDAC1 and 6 we performed docking studies based on a previously reported protocol (see supporting information, Figures S1-S8).[4,17] It was observed that the hindrance imposed by a bulkier cap group allowed the compound to be better accommodated into the HDAC6 enzyme with respect to the HDAC1 isoform. Accordingly, we herein report the docking outputs of **6a** (Figure 3) and **6j** (Figure 4), two of the most selective derivatives of the series with 85- and 140-fold selectivity respectively.

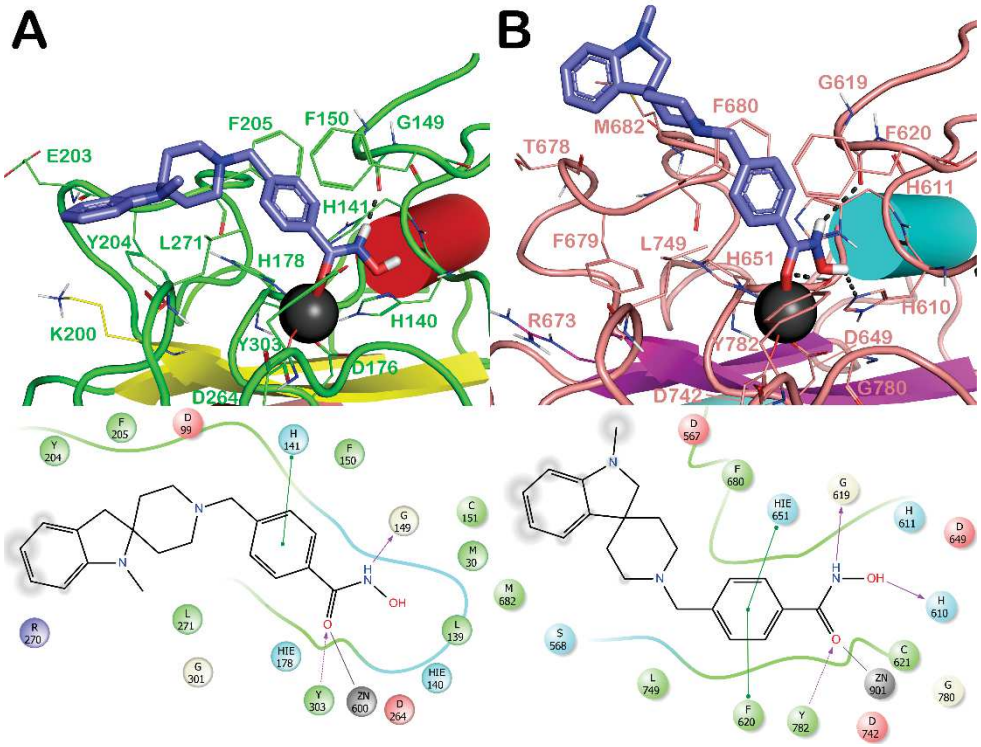

Figure 3. Docked poses of **6a** into HDAC1 (panel A) and HDAC6 (panel B). Compound **6a** is represented by purple sticks while the residues in the active sites are represented by lines and the protein is represented in cartoon form. Zn^{2+} is represented by a gray sphere. H-bonds are shown as by black dotted lines, while the red solid lines represent the metal coordination bonds.

Based on these studies, limited contacts were established by **6a** within the HDAC1 binding site (Figure 3A) compared to the contacts established within the HDAC6 binding site (Figure 3B). In fact, **6a** was able to coordinate with the metal ion in HDAC1 by its hydroxamic moiety through polar contacts with the backbone of G149 and the sidechain of Y303. In addition, we observed only a π-π stacking with H141 and some hydrophobic interactions with Y204, F205 and L271. On the contrary, the docking output of **6a** into HDAC6 showed an improvement of the number of the contacts. In this accommodation, the hydroxamic acid moiety in addition to the metal coordination bond with the Zn^{2+} ion, established a series of supplementary H-bonds with the sidechain of Y782 and H610 and with the backbone of G619. Moreover, the benzyl linker was able to establish a double π-π stacking with F620 and H651. We also noted relevant hydrophobic interactions with F679, F680, M682 and L749. This pattern of interaction perfectly supported the selectivity of **6a** towards HDAC6 over HDAC1 (IC_{50} HDAC1 = 22.4 μM; IC_{50} HDAC6 = 264.4 nM).

Compounds **6b-g** were mainly synthesized in order to investigate the role of the cap-group and its bulkiness on HDAC potency and selectivity, while maintaining unvaried the benzyl moiety of the linker.

Compound **6b**, bearing a pendant benzyl group on the indoline nitrogen of the cap portion, was found to be largely solvent exposed owing to its bulkiness thereby reducing the ligand efficiency. In particular, it showed a π-π stacking with F150 through its benzyl moiety. **6b** showed a decrease of number of the contacts with HDAC6 with the loss of the key π-π stacking with F680 (IC_{50} HDAC1 = 6.5 μM; IC_{50} HDAC6 = 561 nM). The *N*-benzoyl functionality led to a similar pattern of interaction to that described for **6b** with the exclusion

of a π-π stacking with F150. As regards HDAC6, **6c** was able to restore the π-π stacking with F680. Moreover, the carbonyl group belonging to the benzoyl functionality established an H-bond with the sidechain of F680 (IC_{50} HDAC1 = 10.1 μM; IC_{50} HDAC6 = 155 nM). In compound **6d**, the bulk was increased by introducing a phenyl ring on the indoline aromatic moiety, while inserting a methyl group on the indoline nitrogen. Unfortunately, we observed a reduction in hydrophobic contacts as well as a loss of key H-bond interaction, namely with the sidechain of Y303 in HDAC1 and the sidechain of H610 in HDAC6. This pattern accounted for a weak inhibition towards both enzymes with respect to compound **6a** with a percentage of inhibition of 8.5% for HDAC1 and of 50% for HDAC6 when tested at 1 μM. The introduction of a *N*-benzyl moiety as in compound **6d** resulted in the least potent compound of the series. In full agreement with *in vitro* data, the cap group was found completely solvent exposed for both enzymes. Notably, **6f**, bearing a benzoyl group in place of the benzyl of **6e**, was able to establish a H-bond with the backbone of F205 by its carbonyl group. In addition, a strong network of hydrophobic interactions with Y204 and L271 in HDAC1, while an additional π-π stacking with F679 was detected in HDAC6. This accounted for the three-digit nM potency of inhibition of HDAC6 and a μM inhibitory activity for HDAC1 (IC_{50} HDAC6 = 465 nM; IC_{50} HDAC1 = 4.7 μM). In compound **6g** the bioisosteric replacement of the phenyl ring of **6a** with a thiophene led to a decrease in affinity towards both enzymes as already observed by us in the previously reported series of spiroindoline-based HDAC inhibitors.[17]

Based on the computational insights and X-ray co-crystal structure, we synthesized compound **6h** in which we moderately extended the region between the linker and the cap group by replacing the benzyl -CH_2- with a -$COCH_2$- moiety. Moreover, we increased the bulkiness of the cap-group by introducing a pendant benzyl group on the indoline nitrogen. As expected, we observed a slight improvement in the inhibitory potency against both isoforms. In fact, in addition to the contacts found for **6a**, **6h** was able to produce an additional π-π stacking with F205 of HDAC1 through the benzyl functionality. With respect to HDAC6, we observed for the same pattern of interaction for **6h** as already described for **6a** with an additional π-π stacking with F680. This incremental increase in the number of contacts is reflected by an improved inhibitory potency towards both enzymes, although the stronger affinity for HDAC6 was preserved (IC_{50} HDAC1 = 10.2 μM; IC_{50} HDAC6 = 227 nM). Compound **6i** demonstrated that the urea functionality was very well tolerated by both enzymes, as we registered a strong improvement in inhibitory potencies against HDAC1 as well as HDAC6. In the case of HDAC1 enzyme, **6i** established two further interactions relative to those described for **6h**, namely i) an H-bond with the sidechain of H178, and ii) a cation-π stacking with K200. With respect to the HDAC6 enzyme, **6i** interacts with the same residues described for **6h**, displaying an additional H-bond between the sidechain of S568 and the urea NH. This accounts for an increase in inhibitory potency against both enzymes (IC_{50} HDAC1 = 3.6 μM; IC_{50} HDAC6 = 110 nM).

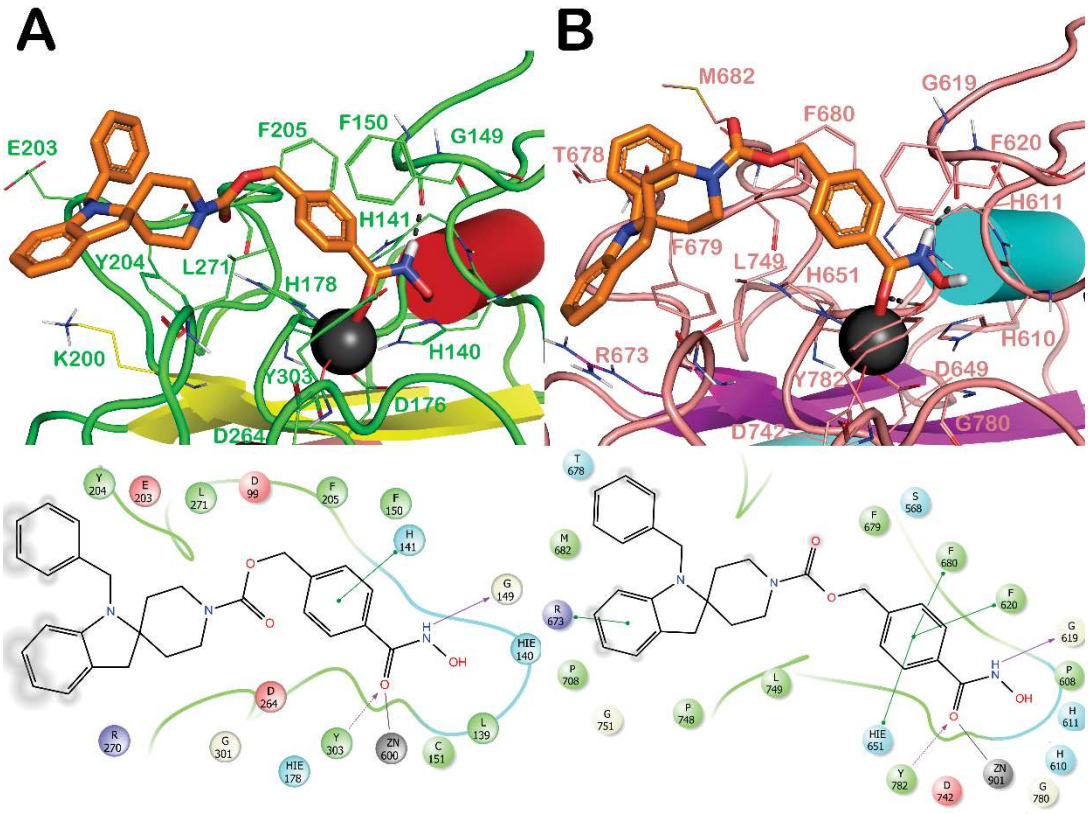

Figure 4. Docked poses of **6j** into HDAC1 (panel A) and HDAC6 (panel B). Compound **6j** is represented by orange sticks while the residues in the active sites are represented by lines and the protein is represented by cartoon. Zn^{2+} is represented by a gray sphere. H-bonds are represented by black dotted lines, while the red lines represent the metal coordination bonds.

Gratifyingly, the introduction of a carbamic functionality to replace the urea moiety led to **6j** that showed a relevant improvement in terms of both potency and selectivity towards HDAC6 over HDAC1. The limited contacts established by **6j** within the HDAC1 binding site (Figure 4A) relative to HDAC6 (Figure 4B) explain the improved potency and selectivity profiles of **6j** over **6a**. Indeed, **6j** was only able to form with HDAC1 the same contacts already described for **6a** without any additional interaction. In addition, the bulkier cap group was found to be largely solvent exposed reducing the ligand efficiency. On the other hand, the docking output of **6j** into HDAC6 showed a huge improvement of the number of the contacts. Its hydroxamic acid moiety in addition to the metal coordination bond with the Zn^{2+} ion, established a series of H-bonds with the sidechain of Y782 and with the backbone of G619. Moreover, for this compound the benzyl linker was able to establish a triple π-π stacking with F620, F680 and H651. Also, relevant hydrophobic interactions with T678, F679, M682 and L749 were observed. Notably, the pendant benzyl group of the cap portion established a cation-π stacking with R673. This pattern of interaction is in strong agreement with the potency and selectivity profile observed for **6j** (IC_{50} *h*HDAC1 = 6.8 μM; IC_{50} *h*HDAC6 = 48 nM; IC_{50} *h*HDAC8 = 3.9 μM). A further computational investigation on **6a** was performed using the crystal structure of *zf*HDAC6 in complex with **6a** in comparison with docking 3D models of **6a** with *h*HDAC6 and *zf*HDAC6. As reported in Figure S9, **6a** accommodated in a similar fashion in both *zf*HDAC6

and *h*HDAC6 enzymes, with only slight differences caused by the different residues within the binding sites. In fact, we noted three main differences in the studied binding sites, the residues D567, T678 and M682 in *h*HDAC6 are replaced by N530, A641 and N645 in *zf*HDAC6. In particular, the presence of M682 in *h*HDAC6 contributed to a slightly different orientation of the cap group that is more solvent exposed with respect to the crystal structure and the docked pose of *zf*HDAC6. However, this study confirms that the *zf*HDAC6 could represent a valuable model for translating the results of potential inhibitors to the *h*HDAC6.
In addition to HDAC1 and 6, the potency of three representative inhibitors (**6a,i,j**, Table 2) was assessed on HDAC8 isoform, which represents a unique member of the class I HDAC family. HDAC8 is endowed with the ability to recognize both histone and non-histone substrates and is ubiquitously expressed and it can localize either in the nucleus or in the cytoplasm.[26] To our delight, the three compounds demonstrated low activity on HDAC8 (from 1.91-3.19 μM, Table 2), thus confirming their significant selective profile towards HDAC6 enzyme.

Table 2. Inhibitory activity of compounds **6a,i,j**, as IC_{50} (μM), against the *h*HDAC8 enzyme

Cpd	**6a**	**6i**	**6j**	**TubA**[17]
IC_{50} (μM)[a]	1.91 ± 0.33	2.48 ± 0.67	3.19 ± 1.51	0.695

[a]All compounds were assayed at least two times, and the results are expressed with standard deviations.

The new molecules were tested in different tumor cell lines which include leukemic and oral and esophageal cancer cells. On the basis of the *in vitro* HDAC affinity and HDAC6 isoform selectivity, the best performing compounds were selected to evaluate their antiproliferative activities. Also, in order to verify their mechanism of action, the target compounds were subjected to cell viability, apoptotic assay (AnnexinV/PI staining), cell cycle analysis (PI staining), cell cycle distribution studies and an analysis of transcription factor activation. Cell cycle distribution and PI analysis studies were performed on U937 and NB4 cell lines, with compounds **6b** and **6h** showing the most promising results. Specifically, in U937 cells, **6h** exhibited cell death and a significant S phase reduction at a concentration of 10 μM compared to the control (DMSO) (as shown in the supporting information, Figure S13). Interestingly, in NB4 cell line, both **6b** and **6h** displayed an identical phenotypic effect in terms of cell death at the two-time intervals 24 and 48 h (Figure 5A,B). Inspired from these results, western blot analyses on NB4 total cell extracts using compounds **6b** and **6h** were performed. Induction of acetylated tubulin was observed (Figure 5C,D), thus confirming HDAC6 inhibition. Moreover, cleavage of PARP at 24 h by **6h** was also detected indicating apoptosis at molecular level at both 24 and 48 h at 10 μM concentration (Fig 5D). Flow cytometry assay of compounds **6a**,**i**,**j** in multiple myeloma cells (U266) showed an induction of apoptotic cell death by these compounds, with compound **6j** resulting the most active (Figure S14).

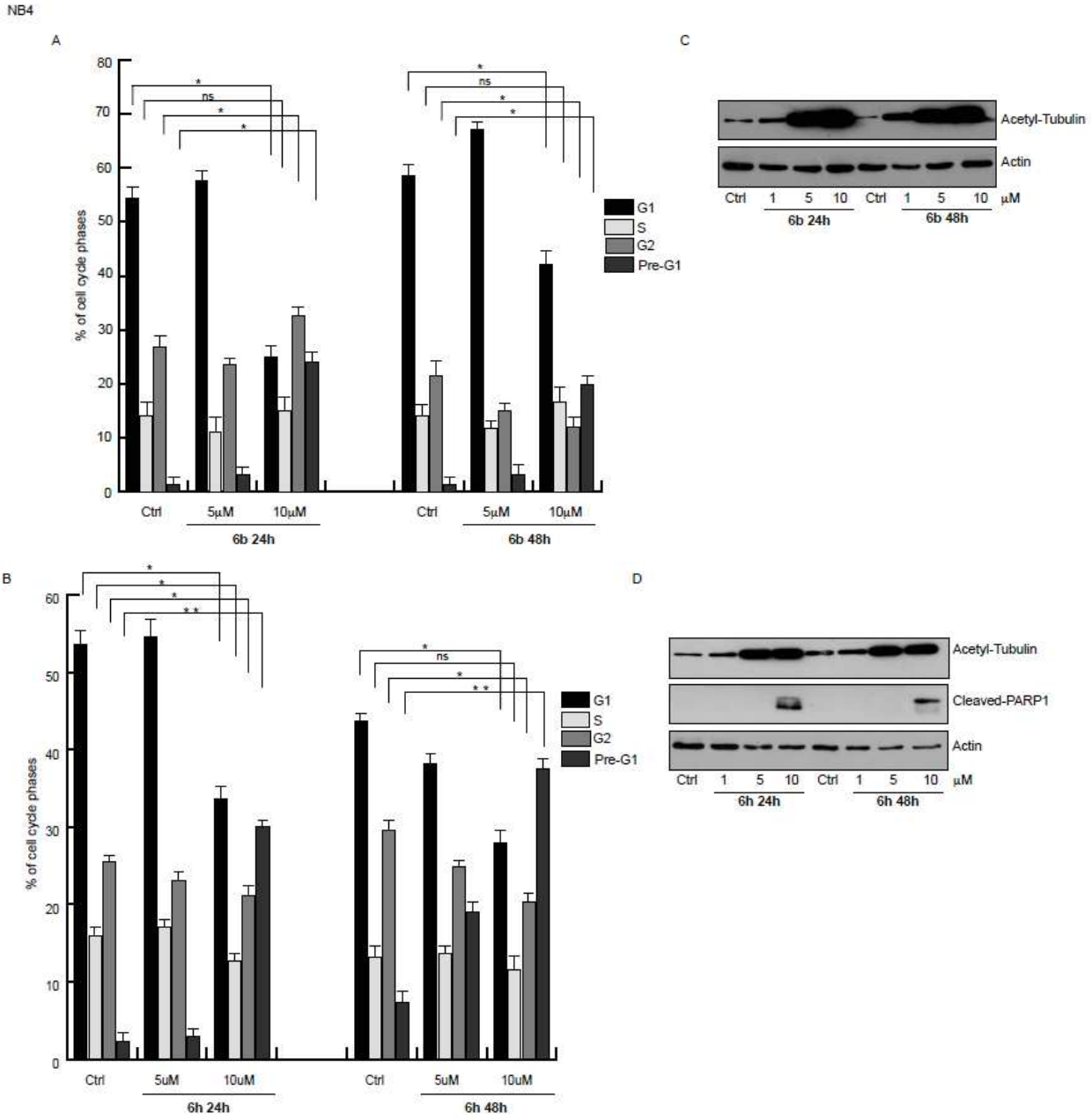

Figure 5. (A, B) FACS analysis of NB4 cells upon **6b** (**A**) and **6h** (**B**) compounds treatment at three different concentrations (1, 5 and 10 μM) at indicated time points. DMSO-treated cells were used as control. Error bars indicate SD of three biological replicates (*$P < 0.05$, **$P \leq 0.01$). (**C, D**). Western blot analysis of NB4 total cell extracts untreated (DMSO) or treated with 1, 5 and 10 μM of 6b (**C**) or 6h (**D**) compounds at indicated times. Immunoblots were performed against the indicated proteins. Actin was used as loading control.

STAT3 represents an important signal transducer and transcription factor displaying a key role in the tumorigenic process. This has been confirmed by the fact that 70% of cancers express activated STAT3.[27] Recent reports highlighting the important crosstalk between HDAC6 and STAT3 have provided deep insights into the mechanistic details regarding cancer therapy. It has been demonstrated that HDAC6 inhibition leads to a decrease in phosphorylated levels of STAT3 and inhibits the expression of STAT3-targeted genes.[28] The enhanced survival of leukemic cells in chronic lymphocytic leukemia and in multiple

myeloma has been associated with the constitutive activation of the JAK/STAT3 signaling pathway.[29,30] Therefore, we proceeded to test STAT3 inhibition using the HDAC6 inhibitors **6a** (prototypic of the new series) and **6j** (most potent HDAC6 inhibitor of the series) at 5 and 10 μM concentration in the human chronic lymphocytic leukemia cell line (MEC1)[31] and at 25 μM against multiple myeloma cells (U266).[32] To our delight, both compounds showed a marked decrease in the levels of pSTAT3 in both cell lines. Specifically, **6j** demonstrated the most potent activity in a dose dependent manner (Figure 6).

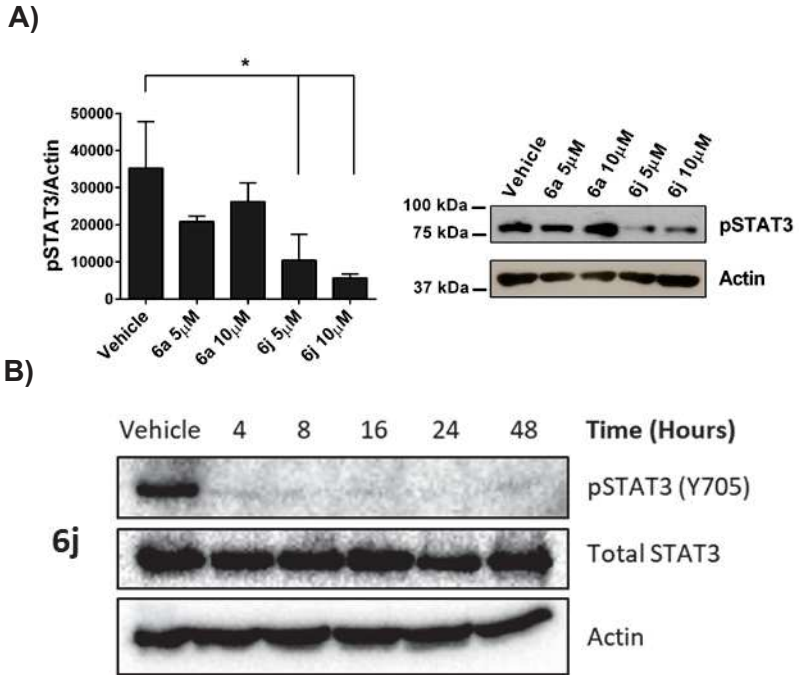

Figure 6. A) Immunoblot analysis of phosphorylated STAT3 in MEC-1 cells treated with **6a** or **6j** (5 μM or 10 μM) for 30 h. Actin was used as loading control. The histogram shows the quantification by densitometric analysis of the levels of phosphorylated STAT3 relative to actin (n = 2). Data are presented as mean value ± SD. One Way ANOVA; *$p < 0.05$; B) Immunoblot analysis of phosphorylated STAT3 in U266 cells treated with **6j** (25 μM) for 4, 8. 16, 24 and 48 h. Cells were collected, lysed and ran on 12% SDS-PAGE.

The majority of cases of oral and esophageal cancer (OEC) are detected late and despite recent medical advances, diagnosis is still relatively poor.[33,34] In a range of malignancies HDAC6 has been found to be over-expressed and shown to correlate with increased tumor aggressiveness[35–38] including oral squamous cell carcinoma[39] and esophageal squamous cell carcinoma.[40] HDAC6 thus represents a key potential target for therapeutic drug development in OEC. The compounds were also screened against several human cancer cell lines namely, KYSE520 (esophageal squamous cell carcinoma), OE33 (esophageal adenocarcinoma), Ca9-22 (gingival squamous cell carcinoma), TR-146 (buccal mucosa squamous cell carcinoma). The results suggested that the selected compounds exhibit antiproliferative activity. **6b** demonstrated the highest activity against KYSE520 (IC_{50} = 12.76 μM), OE33 (IC_{50} = 5.56 μM), Ca9-22 (IC_{50} = 19.00 μM) and TR-146 (IC_{50} = 18.00 μM, Table 3), while **6j**, even if it was the best performing analogue in enzymatic assays, was found less potent in these cell-based assays since, being a carbamate in nature, might be subject to hydrolytic

processes. Flow cytometric analysis established that **6b** was able to trigger apoptosis after 48 h of treatment in KYSE520 cell lines (see supporting information, section 6.1).

Furthermore, cytotoxicity assays were performed on the prototype compound **6a** and the compound with the best activity against cancer cells **6b**, to establish the effect on mouse fibroblasts NIH3T3. The results indicated that the compound **6b** shows a TC_{50} of 40 μM being slightly less toxic than **6a** (TC_{50} of 24 μM, Table 5 SI). Potential mutagenicity caused by the use of hydroxamic-based compounds remains a major concern affecting their drug-like profile.[41] To asses this property Ames test towards two strains of *Salmonella typhimurium* (TA98 and TA100), with and without metabolic activation by employing rat liver S9 fraction, was carried out. It was clear from the results that compounds **6a**,**b** showed no mutagenic effect on the TA98 strain (with or without S9 activation) but low mutagenicity on TA100 strain (above 8 μM for compound **6b** or above 24 to 40 μM for compounds **6a** and **6j** as shown in the supporting information, section 10.1) was detected. This effect has been reported also for FDA approved HDACi (**1**-**4**), and it is mostly supposed to be determined by a Lossen rearrangement involving the hydroxamate group. This process, leads to the generation of the corresponding isocyanate, which can trigger mutagenicity by damaging the DNA due to its susceptibility to undergo nucleophilic attack.[42] Moreover, the capability of HDACi to unwind chromatin may also expose DNA to damage by intracellular factors such as reactive oxygen species (ROS), which can cause further DNA damage leading to genetotoxicity.[43,44]

In summary, a new series of spiroindoline-capped derivatives were developed and characterized as isoform-selective HDAC6 inhibitors. X-ray crystallographic studies on the prototype compound **6a** allowed us to understand its binding mode thus enabling a further rational design of new derivatives aimed at improving potency and selectivity towards HDAC6. Biological evaluation of these compounds led to the identification of **6j** as the most potent and selective HDAC6 inhibitor with an IC_{50} value of 48.5 nM and a selectivity index of 140 over HDAC1 isoform. Further studies on compounds **6a,b,h,j** showed their antiproliferative potential against several cancer cell lines with IC_{50} in the micromolar range. Congruent with their mode of action, **6b** and **6h** induced an increase in acetylated tubulin levels as confirmed using a Western blotting analysis. Moreover, PARP cleavage was observed with compound **6h** indicating its pro-apoptotic potential at the molecular level in NB4 cell extracts. Based on the recent reports highlighting the role of HDAC6 inhibition on the regulation of pSTAT3, we tested the most potent and selective HDAC6 inhibitor from the newly developed series **6j** for STAT3 inhibition. Gratifyingly, **6j** was able to inhibit STAT3 in the MEC1 and U266 cell lines showing a significant decrease in pSTAT3 levels in a dose- and time-dependent manner. In conclusion, the studies here presented on this set of HDAC6 inhibitors contributed to advance our understanding of the structural determinants necessary for potent and selective HDAC6 inhibition and could pave the way for the discovery of novel HDAC6 inhibitors as anticancer agents.

ASSOCIATED CONTENT

Supporting Information

The Supporting Information is available free of charge on the ACS Publications website at DOI:

Supplementary figures, details of the synthetic chemistry, *in silico* studies, and biological assays (PDF)

Accession codes

The atomic coordinates and crystallographic structure factors of the HDAC6 complex with inhibitor **6a** has been deposited in the Protein Data Bank (www.rcsb.org) with accession code 6V7A. Authors will release the atomic coordinates and experimental data upon article publication.

AUTHOR INFORMATION

Corresponding Authors

*(G.C.) E-mail: campiani@unisi.it. Phone: (+39) 0577 232239

Present Addresses

[1]Wellcome Centre for Anti-Infectives Research, Drug Discovery Unit, Division of Biological Chemistry and Drug Discovery, University of Dundee, DD1 5EH Dundee, United Kingdom;

Author Contributions

[#]These authors contributed equally to this work

Funding Sources

This research was supported by European Union's Horizon 2020 (EU) Research and Innovation Programme under the Marie Sklodowska-Curie grant agreement N. 721906 - TRACT and US National Institutes of Health (NIH) grant GM49758. This research was funded also by MIUR20152TE5PK; VALERE: Vanvitelli per la Ricerca; Campania Regional Government Technology Platform Lotta alle Patologie Oncologiche: iCURE; Campania Regional Government FASE2: IDEAL. MIUR, Proof of Concept POC01_00043. This research was funded also by Tuscany strategic project POR-FSE 2014-2020, 'Medicina di Precisione e Malattie Rare'(MePreMaRe), (ACE-ESCC).

Notes

The authors declare no competing financial interests.

ACKNOWLEDGEMENTS

The authors acknowledge support from the European Union's Horizon 2020 (EU) Research and Innovation Programme under the Marie Sklodowska-Curie grant agreement N. 721906. The authors gratefully acknowledge also Cost Action EPICHEMBIO CM1406 (G.C and M.B.) and the synchrotron beamline staff at the Advanced Photon Source (APS) for assistance, especially David Neau. Specifically, we thank the Northeastern Collaborative Access Team (NE-CAT) which is funded by the National Institute of General Medical Sciences (NIGMS) from the NIH (P30 GM124165). The Pilatus 6M detector on beamline 24-ID-C is funded by a NIH-ORIP HEI grant (S10 RR029205). This research used resources of the Advanced Photon Source (APS), a U.S. Department of Energy (DOE) Office of Science User Facility operated for the DOE Office of Science by Argonne National Laboratory under Contract No. DE-AC02-06CH11357. N.R.

gratefully aknowledges Tuscany strategic project POR-FSE 2014-2020, 'Medicina di Precisione e Malattie Rare'(MePreMaRe), (ACE-ESCC).

ABBREVIATIONS

PTM, post-translational modifications; HDAC, histone deacetylase; HDACi, HDAC inhibitors; ZBG, zing binding group; FDA, Food and Drug administration; Hsp90, heat shock protein 90; NaHMDS, sodium bis(trimethylsilyl)amide; THF, tetrahydrofuran; TEA, triethylamine; DCM, dichloromethane; DIPEA, *N*,*N*-diisopropylethylamine; NMO, 4-methylmorpholine *N*-oxide; EDCI, 1-ethyl-3-(3-dimethylaminopropyl)carbodiimide; HOBT, 1-hydroxybenzotriazole hydrate; CDI, 1,1'-carbonyldiimidazole; SAR, structure-activity relationship; OEC, oral and esophageal cancer; KYSE520, esophageal squamous cell carcinoma; OE33, esophageal adenocarcinoma; Ca9-22, gingival squamous cell carcinoma; TR-146, buccal mucosa squamous cell carcinoma; PI, propidium iodide; U937, monocytic leukemia; NB4, acute promyelocytic leukemia; DMSO, dimethyl sulfoxide; PARP, poly (ADP-ribose) polymerase; STAT3, signal transducer and activator of transcription 3; JAK, Janus kinase; MEC1, human chronic lymphocytic leukemia; U266, multiple myeloma cells; NIH3T3, mouse fibroblast; TA98 and TA100, *Salmonella typhimurium strains*; ROS, reactive oxygen species; HNMR, proton nuclear magnetic resonance.

REFERENCES

(1) Portela, A.; Esteller, M. Epigenetic Modifications and Human Disease. *Nat. Biotechnol.* **2010**, *28* (10), 1057–1068. https://doi.org/10.1038/nbt.1685.

(2) Hassig, C. A.; Schreiber, S. L. Nuclear Histone Acetylases and Deacetylases and Transcriptional Regulation: HATs off to HDACs. *Curr. Opin. Chem. Biol.* **1997**, *1* (3), 300–308. https://doi.org/https://doi.org/10.1016/S1367-5931(97)80066-X.

(3) Bertrand, P. Inside HDAC with HDAC Inhibitors. *Eur. J. Med. Chem.* **2010**, *45* (6), 2095–2116. https://doi.org/https://doi.org/10.1016/j.ejmech.2010.02.030.

(4) Brindisi, M.; Cavella, C.; Brogi, S.; Nebbioso, A.; Senger, J.; Maramai, S.; Ciotta, A.; Iside, C.; Butini, S.; Lamponi, S.; Novellino, E.; Altucci, L.; Jung, M.; Campiani, G.; Gemma, S. Phenylpyrrole-Based HDAC Inhibitors: Synthesis, Molecular Modeling and Biological Studies. *Future Med. Chem.* **2016**, *8* (13), 1573–1587. https://doi.org/10.4155/fmc-2016-0068.

(5) Saccoccia, F.; Brindisi, M.; Gimmelli, R.; Relitti, N.; Guidi, A.; Prasanth, A.; Cavella, C.; Brogi, S.; Chemi, G.; Papoff, G.; Herp, D.; Jung, M.; Campiani, G.; Gemma, S.; Ruberti, G. Screening and Phenotypical Characterization of Schistosoma Mansoni Histone Deacetylase 8 (SmHDAC8) Inhibitors as Multi-Stage Antischistosomal Agents Histone Deacetylase 8 (Sm HDAC8) Inhibitors as Multi-Stage Anti- a Institute b Department c Department. *ACS Infect. Dis.* **2020**, *6* (1), 100–113. https://doi.org/10.1021/acsinfecdis.9b00224.

(6) Landucci, E.; Brindisi, M.; Bianciardi, L.; Catania, L. M.; Daga, S.; Croci, S.; Frullanti, E.; Fallerini, C.; Butini, S.; Brogi, S.; Furini, S.; Melani, R.; Molinaro, A.; Lorenzetti, F. C.; Imperatore, V.; Amabile, S.; Mariani, J.; Mari, F.; Ariani, F.; Pizzorusso, T.; Pinto, A. M.; Vaccarino, F. M.; Renieri,

A.; Campiani, G.; Meloni, I. IPSC-Derived Neurons Profiling Reveals GABAergic Circuit Disruption and Acetylated α-Tubulin Defect Which Improves after IHDAC6 Treatment in Rett Syndrome. *Exp. Cell Res.* **2018**, *368* (2), 225–235. https://doi.org/https://doi.org/10.1016/j.yexcr.2018.05.001.

(7) Duvic, M.; Vu, J. Vorinostat: A New Oral Histone Deacetylase Inhibitor Approved for Cutaneous T-Cell Lymphoma. *Expert Opin. Investig. Drugs* **2007**, *16* (7), 1111–1120. https://doi.org/10.1517/13543784.16.7.1111.

(8) Grant, C.; Rahman, F.; Piekarz, R.; Peer, C.; Frye, R.; Robey, R. W.; Gardner, E. R.; Figg, W. D.; Bates, S. E. Romidepsin: A New Therapy for Cutaneous T-Cell Lymphoma and a Potential Therapy for Solid Tumors. *Expert Rev. Anticancer Ther.* **2010**, *10* (7), 997–1008. https://doi.org/10.1586/era.10.88.

(9) Fenichel, M. P. FDA Approves New Agent for Multiple Myeloma. *J. Natl. Cancer Inst.* **2015**, *107* (6), djv165. https://doi.org/10.1093/jnci/djv165.

(10) Poole, R. M. Belinostat: First Global Approval. *Drugs* **2014**, *74* (13), 1543–1554. https://doi.org/10.1007/s40265-014-0275-8.

(11) Gryder, B. E.; Sodji, Q. H.; Oyelere, A. K. Targeted Cancer Therapy: Giving Histone Deacetylase Inhibitors All They Need to Succeed. *Future Med. Chem.* **2012**, *4* (4), 505–524. https://doi.org/10.4155/fmc.12.3.

(12) Mackwitz, M. K. W.; Hamacher, A.; Osko, J. D.; Held, J.; Schöler, A.; Christianson, D. W.; Kassack, M. U.; Hansen, F. K. Multicomponent Synthesis and Binding Mode of Imidazo[1,2-a]Pyridine-Capped Selective HDAC6 Inhibitors. *Org. Lett.* **2018**, *20* (11), 3255–3258. https://doi.org/10.1021/acs.orglett.8b01118.

(13) Brindisi, M.; Saraswati, A. P.; Brogi, S.; Gemma, S.; Butini, S.; Campiani, G. Old but Gold: Tracking the New Guise of Histone Deacetylase 6 (HDAC6) Enzyme as a Biomarker and Therapeutic Target in Rare Diseases. *J. Med. Chem.* **2020**, *63* (1), 23–39. https://doi.org/10.1021/acs.jmedchem.9b00924.

(14) Aldana-Masangkay, G. I.; Sakamoto, K. M. The Role of HDAC6 in Cancer. *Biomed Res. Int.* **2010**, *2011*.

(15) Lahm, A.; Paolini, C.; Pallaoro, M.; Nardi, M. C.; Jones, P.; Neddermann, P.; Sambucini, S.; Bottomley, M. J.; Lo Surdo, P.; Carfí, A.; Koch, U.; De Francesco, R.; Steinkühler, C.; Gallinari, P. Unraveling the Hidden Catalytic Activity of Vertebrate Class IIa Histone Deacetylases. *Proc. Natl. Acad. Sci.* **2007**, *104* (44), 17335 LP – 17340. https://doi.org/10.1073/pnas.0706487104.

(16) Hai, Y.; Shinsky, S. A.; Porter, N. J.; Christianson, D. W. Histone Deacetylase 10 Structure and Molecular Function as a Polyamine Deacetylase. *Nat. Commun.* **2017**, *8* (1), 15368. https://doi.org/10.1038/ncomms15368.

(17) Brindisi, M.; Senger, J.; Cavella, C.; Grillo, A.; Chemi, G.; Gemma, S.; Cucinella, D. M.; Lamponi, S.; Sarno, F.; Iside, C.; Nebbioso, A.; Novellino, E.; Shaik, T. B.; Romier, C.; Herp, D.; Jung, M.; Butini, S.; Campiani, G.; Altucci, L.; Brogi, S. Novel Spiroindoline HDAC Inhibitors: Synthesis, Molecular Modelling and Biological Studies. *Eur. J. Med. Chem.* **2018**, *157*, 127–138.

https://doi.org/https://doi.org/10.1016/j.ejmech.2018.07.069.

(18) Hai, Y.; Christianson, D. W. Histone Deacetylase 6 Structure and Molecular Basis of Catalysis and Inhibition. *Nat. Chem. Biol.* **2016**, *12* (9), 741–747. https://doi.org/10.1038/nchembio.2134.

(19) Gemma, S.; Gabellieri, E.; Sanna Coccone, S.; Martí, F.; Taglialatela-Scafati, O.; Novellino, E.; Campiani, G.; Butini, S. Synthesis of Dihydroplakortin, 6-Epi-Dihydroplakortin, and Their C10-Desethyl Analogues. *J. Org. Chem.* **2010**, *75* (7), 2333–2340. https://doi.org/10.1021/jo1001559.

(20) Liu, K. G.; Robichaud, A. J.; Lo, J. R.; Mattes, J. F.; Cai, Y. Rearrangement of 3,3-Disubstituted Indolenines and Synthesis of 2,3-Substituted Indoles. *Org. Lett.* **2006**, *8* (25), 5769–5771. https://doi.org/10.1021/ol0623567.

(21) Campiani, G.; Fiorini, I.; De Filippis, M. P.; Ciani, S. M.; Garofalo, A.; Nacci, V.; Giorgi, G.; Sega, A.; Botta, M.; Chiarini, A.; Budriesi, R.; Bruni, G.; Romeo, M. R.; Manzoni, C.; Mennini, T. Cardiovascular Characterization of Pyrrolo[2,1-d][1,5]Benzothiazepine Derivatives Binding Selectively to the Peripheral-Type Benzodiazepine Receptor (PBR): From Dual PBR Affinity and Calcium Antagonist Activity to Novel and Selective Calcium Entry Blocke. *J. Med. Chem.* **1996**, *39* (15), 2922–2938. https://doi.org/10.1021/jm960162z.

(22) Hai, Y.; Christianson, D. W. Histone Deacetylase 6 Structure and Molecular Basis of Catalysis and Inhibition. *Nat. Chem. Biol.* **2016**, *12* (9), 741–747. https://doi.org/10.1038/nchembio.2134.

(23) Osko, J. D.; Porter, N. J.; Narayana Reddy, P. A.; Xiao, Y.-C.; Rokka, J.; Jung, M.; Hooker, J. M.; Salvino, J. M.; Christianson, D. W. Exploring Structural Determinants of Inhibitor Affinity and Selectivity in Complexes with Histone Deacetylase 6. *J. Med. Chem.* **2020**, *63* (1), 295–308. https://doi.org/10.1021/acs.jmedchem.9b01540.

(24) Porter, N. J.; Osko, J. D.; Diedrich, D.; Kurz, T.; Hooker, J. M.; Hansen, F. K.; Christianson, D. W. Histone Deacetylase 6-Selective Inhibitors and the Influence of Capping Groups on Hydroxamate-Zinc Denticity. *J. Med. Chem.* **2018**, *61* (17), 8054–8060. https://doi.org/10.1021/acs.jmedchem.8b01013.

(25) Bhatia, S.; Krieger, V.; Groll, M.; Osko, J. D.; Reßing, N.; Ahlert, H.; Borkhardt, A.; Kurz, T.; Christianson, D. W.; Hauer, J.; Hansen, F. K. Discovery of the First-in-Class Dual Histone Deacetylase–Proteasome Inhibitor. *J. Med. Chem.* **2018**, *61* (22), 10299–10309. https://doi.org/10.1021/acs.jmedchem.8b01487.

(26) Chakrabarti, A.; Oehme, I.; Witt, O.; Oliveira, G.; Sippl, W.; Romier, C.; Pierce, R. J.; Jung, M. HDAC8: A Multifaceted Target for Therapeutic Interventions. *Trends Pharmacol. Sci.* **2015**, *36* (7), 481–492. https://doi.org/10.1016/j.tips.2015.04.013.

(27) Frank, D. A. STAT3 as a Central Mediator of Neoplastic Cellular Transformation. *Cancer Lett.* **2007**, *251* (2), 199–210. https://doi.org/https://doi.org/10.1016/j.canlet.2006.10.017.

(28) Keremu, A.; Aimaiti, A.; Liang, Z.; Zou, X. Role of the HDAC6/STAT3 Pathway in Regulating PD-L1 Expression in Osteosarcoma Cell Lines. *Cancer Chemother. Pharmacol.* **2019**, *83* (2), 255–264. https://doi.org/10.1007/s00280-018-3721-6.

(29) Hazan-Halevy, I.; Harris, D.; Liu, Z.; Liu, J.; Li, P.; Chen, X.; Shanker, S.; Ferrajoli, A.; Keating, M. J.; Estrov, Z. STAT3 Is Constitutively Phosphorylated on Serine 727 Residues, Binds DNA, and Activates Transcription in CLL Cells. *Blood* **2010**, *115* (14), 2852–2863. https://doi.org/10.1182/blood-2009-10-230060.

(30) Catlett-Falcone, R.; Landowski, T. H.; Oshiro, M. M.; Turkson, J.; Levitzki, A.; Savino, R.; Ciliberto, G.; Moscinski, L.; Fernández-Luna, J. L.; Nuñez, G.; Dalton, W. S.; Jove, R. Constitutive Activation of Stat3 Signaling Confers Resistance to Apoptosis in Human U266 Myeloma Cells. *Immunity* **1999**, *10* (1), 105–115. https://doi.org/10.1016/S1074-7613(00)80011-4.

(31) Stacchini, A.; Aragno, M.; Vallario, A.; Alfarano, A.; Circosta, P.; Gottardi, D.; Faldella, A.; Rege-Cambrin, G.; Thunberg, U.; Nilsson, K.; Caligaris-Cappio, F. MEC1 and MEC2: Two New Cell Lines Derived from B-Chronic Lymphocytic Leukaemia in Prolymphocytoid Transformation. *Leuk. Res.* **1999**, *23* (2), 127–136. https://doi.org/https://doi.org/10.1016/S0145-2126(98)00154-4.

(32) Nelson, E. A.; Walker, S. R.; Kepich, A.; Gashin, L. B.; Hideshima, T.; Ikeda, H.; Chauhan, D.; Anderson, K. C.; Frank, D. A. Nifuroxazide Inhibits Survival of Multiple Myeloma Cells by Directly Inhibiting STAT3. *Blood* **2008**, *112* (13), 5095–5102. https://doi.org/10.1182/blood-2007-12-129718.

(33) Napier, K. J.; Scheerer, M.; Misra, S. Esophageal Cancer: A Review of Epidemiology, Pathogenesis, Staging Workup and Treatment Modalities. *World J. Gastrointest. Oncol.* **2014**, *6* (5), 112.

(34) Moore, K. A.; Ford, P. J.; Farah, C. S. Support Needs and Quality of Life in Oral Cancer: A Systematic Review. *Int. J. Dent. Hyg.* **2014**, *12* (1), 36–47. https://doi.org/10.1111/idh.12051.

(35) Lernoux, M.; Schnekenburger, M.; Dicato, M.; Diederich, M. Anti-Cancer Effects of Naturally Derived Compounds Targeting Histone Deacetylase 6-Related Pathways. *Pharmacol. Res.* **2018**, *129*, 337–356. https://doi.org/https://doi.org/10.1016/j.phrs.2017.11.004.

(36) Bradbury, C. A.; Khanim, F. L.; Hayden, R.; Bunce, C. M.; White, D. A.; Drayson, M. T.; Craddock, C.; Turner, B. M. Histone Deacetylases in Acute Myeloid Leukaemia Show a Distinctive Pattern of Expression That Changes Selectively in Response to Deacetylase Inhibitors. *Leukemia* **2005**, *19* (10), 1751–1759. https://doi.org/10.1038/sj.leu.2403910.

(37) Bazzaro, M.; Lin, Z.; Santillan, A.; Lee, M. K.; Wang, M.-C.; Chan, K. C.; Bristow, R. E.; Mazitschek, R.; Bradner, J.; Roden, R. B. S. Ubiquitin Proteasome System Stress Underlies Synergistic Killing of Ovarian Cancer Cells by Bortezomib and a Novel HDAC6 Inhibitor. *Clin. Cancer Res.* **2008**, *14* (22), 7340 LP – 7347. https://doi.org/10.1158/1078-0432.CCR-08-0642.

(38) Kanno, K.; Kanno, S.; Nitta, H.; Uesugi, N.; Sugai, T.; Masuda, T.; Wakabayashi, G.; Maesawa, C. Overexpression of Histone Deacetylase 6 Contributes to Accelerated Migration and Invasion Activity of Hepatocellular Carcinoma Cells. *Oncol. Rep.* **2012**, *28* (3), 867–873. https://doi.org/10.3892/or.2012.1898.

(39) Sakuma, T.; Uzawa, K.; Onda, T.; Shiiba, M.; Yokoe, H.; Shibahara, T.; Tanzawa, H. Aberrant Expression of Histone Deacetylase 6 in Oral Squamous Cell Carcinoma. *Int. J. Oncol.* **2006**, *29* (1), 117–124. https://doi.org/10.3892/ijo.29.1.117.

(40) Cao, J.; Lv, W.; Wang, L.; Xu, J.; Yuan, P.; Huang, S.; He, Z.; Hu, J. Ricolinostat (ACY-1215) Suppresses Proliferation and Promotes Apoptosis in Esophageal Squamous Cell Carcinoma via MiR-30d/PI3K/AKT/MTOR and ERK Pathways. *Cell Death Dis.* **2018**, *9* (8), 817. https://doi.org/10.1038/s41419-018-0788-2.

(41) Skipper, P. L.; Tannenbaum, S. R.; Thilly, W. G.; Furth, E. E.; Bishop, W. W. Mutagenicity of Hydroxamic Acids and the Probable Involvement of Carbamoylation. *Cancer Res.* **1980**, *40* (12), 4704 LP – 4708.

(42) Shen, S.; Kozikowski, A. P. Why Hydroxamates May Not Be the Best Histone Deacetylase Inhibitors—What Some May Have Forgotten or Would Rather Forget? *ChemMedChem* **2016**, *11* (1), 15–21. https://doi.org/10.1002/cmdc.201500486.

(43) Brodská, B.; Holoubek, A. Generation of Reactive Oxygen Species during Apoptosis Induced by DNA-Damaging Agents and/or Histone Deacetylase Inhibitors. *Oxid. Med. Cell. Longev.* **2011**, *2011*, 253529. https://doi.org/10.1155/2011/253529.

(44) Miles, M. A.; Harris, M. A.; Hawkins, C. J. Proteasome Inhibitors Trigger Mutations via Activation of Caspases and CAD, but Mutagenesis Provoked by the HDAC Inhibitors Vorinostat and Romidepsin Is Caspase/CAD-Independent. *Apoptosis* **2019**, *24* (5), 404–413. https://doi.org/10.1007/s10495-019-01543-x.